

Modeling of Hysteresis Current Control Technique for Three Phase PV Based VSI using MATLAB/Simulink.

Ashwini Seetharamaiah¹, Jayakumar N²

¹ PG scholar , Dept. of Electrical Engineering, The Oxford College of Engineering, Karnataka, India.

² Associate Professor, Dept. of Electrical Engineering, The Oxford College of Engineering, Karnataka, India.

Abstract - Photovoltaic (PV) cells are the novel and efficient energy converting system at atomic level. In this work the modeling and simulation of photovoltaic based three phase Voltage Source Inverter (VSI) has been carried out. The significance of Boost Converter, Maximum Power Point Tracking (MPPT) and the VSI has been the major aspects of the work. For the maximum extraction of power an intelligent Fuzzy Logic Control (FLC) algorithm is utilized. This paper describes a Phase Locked Loop (PLL)-less hysteresis current control technique for the PV based three phase VSI. Boost Converter is used as an interconnection between the PV module and the inverter, which operates in the continuous conduction mode (CCM). The proposed system is designed and simulated in MATLAB/Simulink environment.

Key Words: Photovoltaic, Voltage Source Inverter, Maximum Power Point Tracking, Boost Converter, Fuzzy Logic Control, PLL-less hysteresis current control.

1. INTRODUCTION

Photovoltaic energy generation is rapidly increasing in demand due to its fusion of various advantages: no fuel cost, pollution-less, maintenance less, no moving parts and lack of audible noise [1]. PV installations on small scale are very popular in remote areas and developing countries as lighting and water pumping solutions. Such PV systems are also used in developed countries with appreciable amount of solar radiation [2]. They could be installed in residential or commercial buildings in order to meet full or partial load demand. If in case the power generated by PV system is more than the load demand then the excess power can be fed back to the grid [3]. However, the major limitations faced in developing a grid connected PV system are –price of PV module and consolidating PV inverter with the grid [4] [5]. The voltage generated from PV array is DC thus an inverter is necessary for the conversion of DC voltage to AC before it is being connected to grid. Grid can be considered as voltage source of infinite efficiency. The output voltage as well as the frequency of inverter should be similar as of grid voltage and frequency. The grid connected inverter output can be controlled either as a current or voltage source inverter. Pulse width modulated (PWM) VSI are widely in use in PV systems. Thus it is necessary to utilize the energy generated by PV

module ideally. For the optimum use of PV module a proper MPPT algorithm has to be adopted so as to maximize the extraction of solar power under varying insolation and temperature conditions. Here a fuzzy logic based control algorithm has been selected. The efficient working of the grid connected VSI depends on the control strategy that should be able to withstand most adverse conditions like fluctuations in voltage and frequency. This paper illustrates hysteresis current control (HCC) technique without PLL for providing a faster response. The superior purpose of this control approach is that the derivation of fundamental components of load currents, calculation of in-phase and quadrature unit templates, calculation of AC and DC loss components and computation of the reference grid currents. The entire proposed system is portrayed in Fig-1. The system has been simulated in MATLAB/Simulink environment.

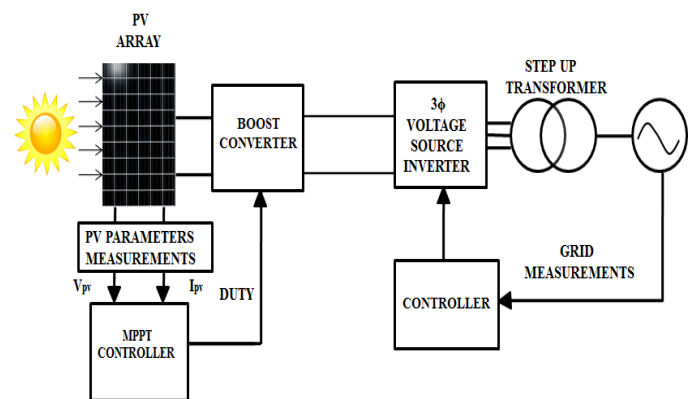


Fig -1: Block diagram of the proposed system

As seen from Fig-1. The PV array is connected to DC-DC converter. The switching signals for DC-DC converter is generated by fuzzy logic control based MPPT. By using feedback voltage and power taken from the PV array, fuzzy logic control based MPPT produces a reference for the converter.

2. MATHEMATICAL MODELING OF PVM

For the analysis of PV system connected to the grid it is extremely important to model the PV module. Certain parameters are not available in the datasheet. Such parameters are estimated by utilizing the available parameters from the manufacturer's datasheet. Basically a

PV cell is a p-n junction semiconductor device. It can be compared to a current generator with voltage dependent source. The theoretical and equivalent circuit of a PV cell is illustrated in Fig-2. The prevalence of light on the cell propagates charge carriers that generate an electric current granted that the cell is short-circuited [6].

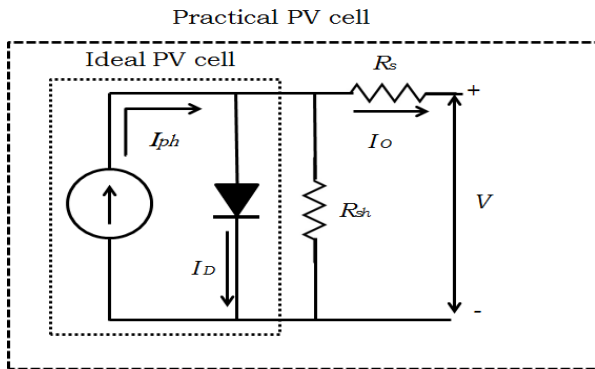


Fig -2: Theoretical and equivalent circuit of PV cell

In the above circuit the bypass diode assume the role of a p-n junction. It protects PV cell in distinction of overheating in the course of partial shading. \$R_s\$ correspond to series resistance and \$R_{sh}\$ is the parallel resistance. In this proposed work, \$R_{sh}\$ is undervalued in order to simplify the calculation [7].

Using MATLAB/Simulink the PV module is modeled employing the mathematical equations. A bit-by-bit model buildup is explained below:

The PV cell current \$I_o\$ is formulated by the following equation,

$$I_o = N_p I_{ph} - N_p I_D \left[e^{\left\{ \frac{q(V_{oc} + I_o R_s)}{N_s A K T_{ak}} \right\}} - 1 \right] \quad \dots\dots (1)$$

Where, \$N_p\$ is number of cells connected in parallel (here, \$N_p = 1\$); \$q\$ is electron charge (\$q = 1.69 \times 10^{-19} C\$); \$V_{oc}\$ is the open-circuit voltage \$N_s\$ is the number of cells connected in series (here, \$N_s = 32\$); \$T_{ak}\$ is module operating temperature; \$A\$ is the ideality factor (\$A = 1.2\$); \$K\$ is the Boltzmann's constant (\$K = 1.381 \times 10^{-23} J/K\$); \$I_{ph}\$ is the photocurrent and \$I_D\$ is diode current expressed by,

$$I_{ph} = [I_{scr} + \{k_i \times (T_{ak} - T_{rk})\}] \times \frac{S}{1000} \quad \dots\dots (2)$$

Where, \$I_{scr}\$ is PV module short circuit current at 25°C; \$k_i\$ is the temperature co-efficient at \$I_{scr} = 0.0013A/°C\$; \$T_{rk}\$ is reference temperature; \$S\$ is the illumination on PV module (\$S = 1000W/cm^2\$).

$$I_D = I_{rr} \left(\frac{T_{ak}}{T_{rk}} \right)^3 \left[e^{\left\{ \frac{q E_g}{K A} \left(\frac{1}{T_{rk}} - \frac{1}{T_{ak}} \right) \right\}} \right] \quad \dots\dots (3)$$

Where, \$E_g\$ is band gap of Si (1.12eV); \$I_{rr}\$ is the reverse saturation current formulated as:

$$I_{rr} = I_{scr} / \left[e^{\left\{ \frac{q V_{oc}}{K N_s A T_{rk}} \right\}} \right] \quad \dots\dots (4)$$

Table -1: Parameters available in the manufacture's datasheet (PdtId. 120 H24, Maharishi Solar, India)

Attributes	Values
\$I_{SCR}\$	3.82A
\$V_{OC}\$	44.11V
\$V_{MPP}\$	35.62V
\$I_{MPP}\$	3.595A
\$P_{MPP}\$	128.1W

The Simulink model of PVM is depicted in Fig-3.

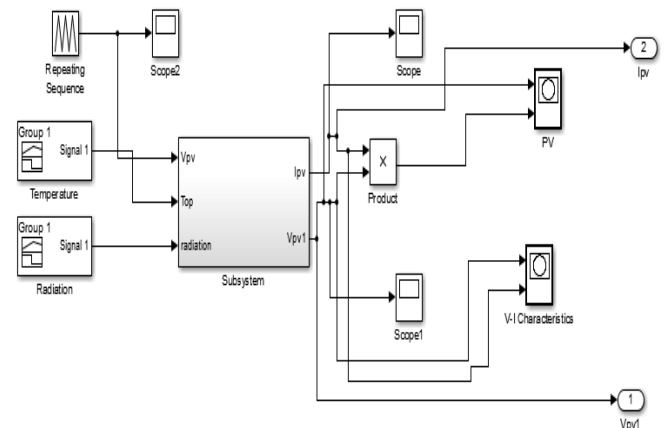


Fig -3: Simulink model of PV module

3. FUZZY LOGIC BASED MPPT CONTROL

3.1 Maximum Power Point tracking:

The output power from solar panel fluctuates with the temperature and irradiation. On the other hand for a particular operating case we obtain a curve that gives particular voltage value preserved by the solar panel for a particular current value. Such a plot is termed as characteristics curve. PV panels have unique I-V (current v/s voltage) and P-V (power v/s voltage) characteristics as interpreted in Fig-4.

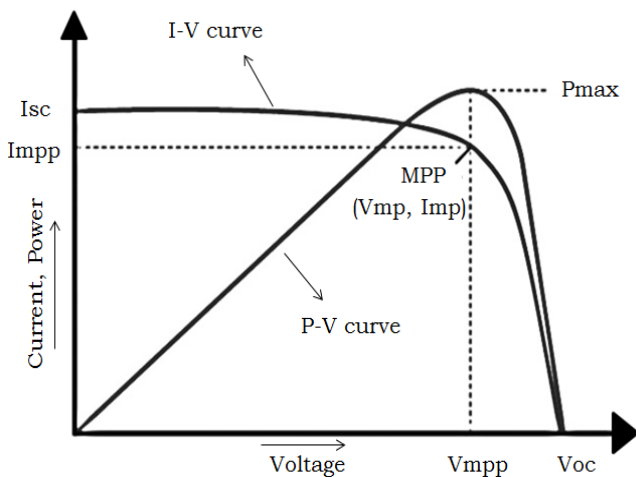


Fig -4: (I-V) and (P-V) characteristics

PV panels have very low-lying conversion efficiency about 15 percent for the manufactured panels. This efficiency reduces remarkably due to irradiation, temperature and load conditions. Therefore from the characteristics of solar panel it is decisive to operate PV panels at maximum power point (MPP) to boost PV panel or module efficiency. Hence it becomes mandatory to track the MPP so that we obtain maximum efficiency from PV panel. This technique is described as Maximum Power Point Tracking (MPPT).

3.2 Fuzzy Logic MPPT controllers:

As a result of tremendous developments in the areas of microcontroller and DSP technologies FLC has gained much interest in MPPT applications. Fuzzy logic Controller is a non-linear control technique [8]. It adopts fuzzy logics to frame decisions for controlling the output of the controller [9]. The vital utility of FLC is owing to its operations under unpredictability conditions like change in weather, temperature and insolation. It does not require a detailed dynamic model of the system and can work with imperfect inputs. Thus it is feasible to adapt it for non-linear characteristics of PV panel to trace the maximum power point [10]. Furthermore FLC has excellent accuracy with regard to tracking and improved robustness as compared to other hill climbing techniques [11].

The FLC used for the MPPT includes the following components: Fuzzification process, Rule base, Inference and defuzzification process. The major configuration of FLC based MPPT is portrayed in Fig-5 and the components are explained in detail below:

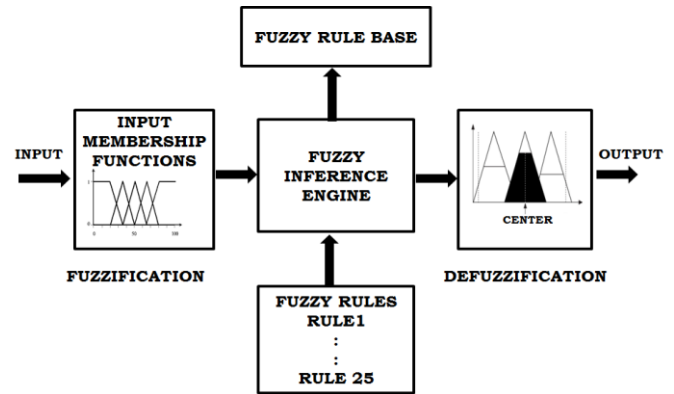


Fig -5: Major configuration of fuzzy logic controller

Fuzzification process involves the determination of the input values from the prescribed fuzzy sets through membership functions. The fuzzy inference is provided with two inputs labelled as error (e) and change in error (Δe) which is accomplished by the following set of equations at a sampling instant, i (say).

$$Error, e(i) = \frac{\Delta P_{pv}}{\Delta V_{pv}} = \frac{P(i) - P(i-1)}{V(i) - V(i-1)} \quad \dots\dots\dots (5)$$

$$Change\ in\ error, \Delta e(i) = e(i) - e(i - 1) \quad \dots\dots\dots (6)$$

The $e(i)$ specify the position of operating point on the P-V curve at an instant, i which may be on left or right side of MPP. While the $\Delta e(i)$ gives rearrangement of the operating point with reference to MPP. The linguistic variables considered in this task are Massive Negative (MN), Intermediate Negative (IN), Tiny Negative (TN), Zero Error (ZE), Massive Positive (MP), Intermediate Positive (IP) and Tiny Positive (TP) (Li and Wang, 2009). In this proposed work error ranges from -200W/A to 200W/A while the change in error ranges from -100W/A to 100W/A. Based on the number of inputs, rules are framed in parallel and the order in which rules are placed is completely unimportant. Table -2 depicts the rule base table. The table provides 25 control rules for resolving fuzzy output (here it is duty ratio).

Table -2: Rule base for the MPPT controller

$e \backslash \Delta e$	MP	IP	TP	ZE	TN	IN	MN
MN	ZE	TN	IN	MN	MN	MN	MN
IN	TP	ZE	TN	IN	MN	MN	MN
TN	IP	TP	ZE	TN	IN	MN	MN
ZE	MP	IP	TP	ZE	TN	IN	MN
TP	MP	MP	IP	TP	ZE	TN	IN
IP	MP	MP	MP	IP	TP	ZE	TN
MP	MP	MP	MP	MP	IP	TP	ZE

Inference is a process of evaluating the scaling from a received input to output using fuzzy logics. The scaling then serves a basis from which the decisions can be implemented. The rule base statements are utilized in this phase. In this work simple Madmani-type Fuzzy Inference System (FIS) is considered.

In the defuzzification the fuzzy set is fed as input to the defuzzification process and the output is a distinct number. The ultimate and prominent defuzzification method is the centroid estimation wherein the center of area under the curve is re-established. There are five in-built programs supported: bisector, centroid, middle of maximum, largest of maximum and smallest of maximum.

The duty cycle gained is in addition scaled and supplied to DC-DC converter to monitor the switch via gate pulses. Δd is calculated as follows:

$$\Delta d = \frac{\sum_{k=1}^n \mu(\Delta d_k) \times \Delta d_k}{\sum_{k=1}^n \mu(\Delta d_k)} \quad \text{..... (7)}$$

After defuzzification process the duty cycle is even more scaled as former and supplied to DC-DC converter in accordance with the following equation:

$$d(i) = d(i - 1) + K_d \Delta d(k) \quad \text{..... (8)}$$

Where K_d is the gain as scaling factor for duty cycle ranging from 0.1 to 0.5.

4. DC-DC CONVERTER

The PV system's optimum operating point depends upon the load curve. The maximum power that possibly delivered to load relies upon the optimum value of resistive load. If load varies likewise output power varies too. Thus DC-DC boost converter topology is incorporated between PV panel and load to overcome the unwanted PV power fluctuations. This however maximizes the power transfer fed to load from PV system. It also acts as an impedance adapter for ensuring the synchronization of load impedance with changing PV power [12].

Boost converter bears two conduction modes: continuous conduction mode (CCM) where the inductor current does not reach zero thereby giving productive conversion of power and discontinuous conduction mode (DCM) where the inductor current is allowed to reach zero causing low power conversion. The boost converter arrangement is as shown in the Fig-7.

It consists of two operating states: switch (S_w) in ON state and in OFF state. During S_w is in ON state i.e. closed the current flowing through boost converter that is inductor i_L increments in a linear way and the diode is reverse biased. Meanwhile inductor also starts storing energy. During S_w is in OFF state i.e. opened the energy

stored in the inductor is discharged via diode to the output. Here the boost converter is designed to work in the CCM.

If S_w is in ON state the voltage across the inductor L_1 as well as the DC link can be formulated using the equations given below [13]:

$$L_1 \frac{di_{L1}}{dt} = V_{pv} - V_{dc} \quad \text{..... (9)}$$

$$C \frac{dV_{DC}}{dt} = i_{L1} - \frac{V_{dc}}{R} \quad \text{..... (10)}$$

If S_w is in OFF state then the below equations are applicable:

$$L_1 \frac{di_{L1}}{dt} = V_{pv} \quad \text{..... (11)}$$

$$C \frac{dV_{DC}}{dt} = i_c \quad \text{..... (12)}$$

Where, R indicates the resistive load.

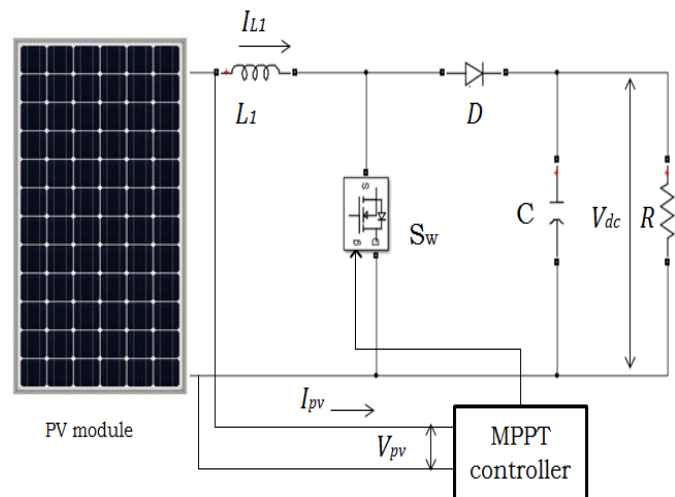


Fig -6: PV fed boost converter

5. VOLTAGE SOURCE INVERTER

An inverter belongs to a group of power conversion circuits converting dc (direct current) to ac (alternating current). It is vital to retain the sustained flow of good power quality supply to the distribution network [14]. This necessitates for an efficient control technique for operating the inverter switches [15]. In view of this proposed work a HCC technique which avoids a PLL has been approached. The control scheme [16] for reference is represented in Fig. 8.

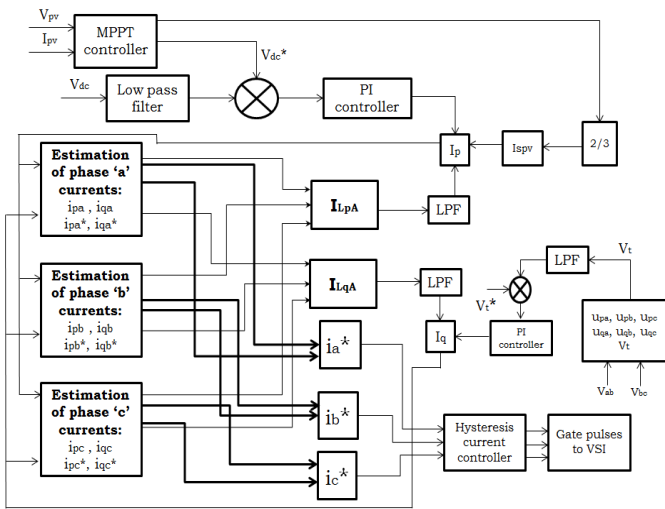


Fig -7: Control scheme of the proposed work

The details of the technique are outlined as below:

The major objectives of proposed control technique are the estimation of: fundamental components of load currents, in-phase and quadrature unit templates, ac and dc loss components and the reference grid currents. From there on to generate the gate pulses the reference grid currents and sensed grid currents are moved onward to the current error extractor and the hysteresis regulator for operating the VSI. MATLAB/Simulink has been used as a tool to implement these equations.

5.1 Computation of unit templates and amplitude of terminal voltages:

By making use of the sensed line voltages (V_{ab} and V_{bc}) from the Power Control Centre (PCC) the phase voltages (V_a, V_b, V_c) are derived from the following equation [17] as:

$$V_a = \frac{2V_{ab} + V_{bc}}{3} \dots\dots (13)$$

$$V_b = \frac{-V_{ab} + V_{bc}}{3} \dots\dots (14)$$

$$V_c = \frac{-V_{ab} - 2V_{bc}}{3} \dots\dots (15)$$

The following list of equations gives:

- Amplitude of terminal voltage:

$$V_t = \sqrt{\frac{2}{3}(V_a^2 + V_b^2 + V_c^2)} \dots\dots (16)$$

- In-phase unit template:

$$u_{pa} = \frac{V_a}{V_t} \dots\dots (17)$$

$$u_{pb} = \frac{V_b}{V_t} \dots\dots (18)$$

$$u_{pc} = \frac{V_c}{V_t} \dots\dots (19)$$

- Quadrature unit templates:

$$u_{qa} = -\frac{u_{pb}}{\sqrt{3}} + \frac{u_{pc}}{\sqrt{3}} \dots\dots (20)$$

$$u_{qb} = \frac{\sqrt{3}u_{pa}}{2} + \frac{(u_{pb} - u_{pc})}{2\sqrt{3}} \dots\dots (21)$$

$$u_{qc} = -\frac{\sqrt{3}u_{pa}}{2} + \frac{(u_{pb} - u_{pc})}{2\sqrt{3}} \dots\dots (22)$$

The implementations of in-phase and quadrature unit templates are shown in Fig-8 and Fig-9.

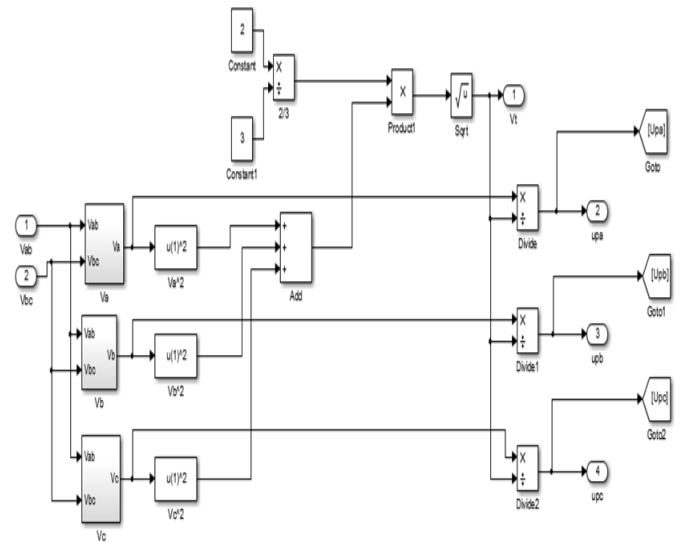


Fig -8: In-phase unit template implementation

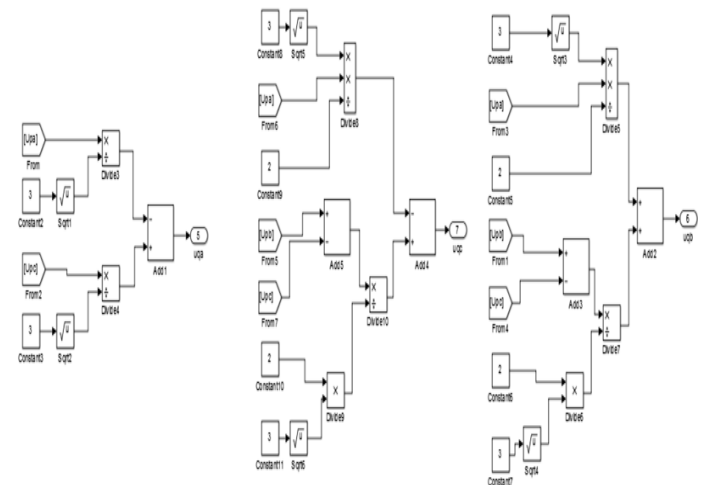


Fig -9: Implementation of quadrature unit template

5.2 Computation of AC and DC components and feed forward term:

- Voltage error:

After the evaluation of terminal voltage (V_t), of the PCC voltage and the terminal reference voltage value (V_t^*) is supplied to a PI controller. At n^{th} instant or sample the error is estimated by the following equation:

$$V_{te}(n) = V_t^*(n) - V_t(n) \quad \dots\dots\dots (23)$$

- AC loss component:

The output from the voltage PI controller is the AC loss component (I_{cq}). This is exercised to sustain the voltage at the PCC.

$$I_{cq}(n + 1) = I_{cq}(n) + K_{pt}(V_{te}(n + 1) - V_{te}(n)) + K_{it}V_{te}(n + 1) \quad \dots\dots\dots (24)$$

Where, K_{it} is the integral gain and K_{pt} is the proportional gain utilized in PI controller.

The MATLAB/Simulink model for the AC loss component is presented is in Fig-10.

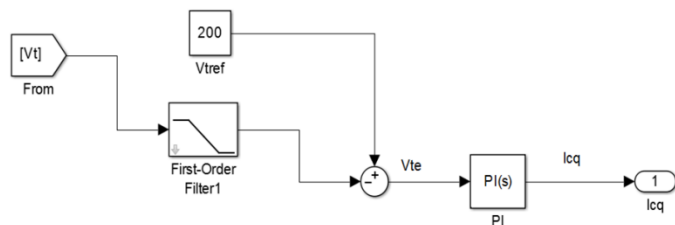


Fig -10: AC loss component generator

- DC link error voltage:

The voltage error of DC link (V_{de}) is evaluated as the change between the reference DC link voltage (V_{dc}^*) value attained from the MPPT and DC link voltage (V_{dc}) sensed as:

$$V_{de}(n) = V_{dc}^*(n) - V_{dc}(n) \quad \dots\dots\dots (25)$$

- DC loss component:

The calculated V_{de} is provided as input to the voltage PI controller and the end product is the DC loss component (I_{cp}) which standardizes the DC link voltage is evaluated as:

$$I_{cp}(n + 1) = I_{cp}(n) + K_{pd}(V_{de}(n + 1) - V_{de}(n)) + K_{id}V_{de}(n + 1) \quad \dots\dots\dots (26)$$

Where, K_{id} and K_{pd} are the integral and proportional gains included in PI controller.

The model representation for DC loss is as shown in Fig-11.

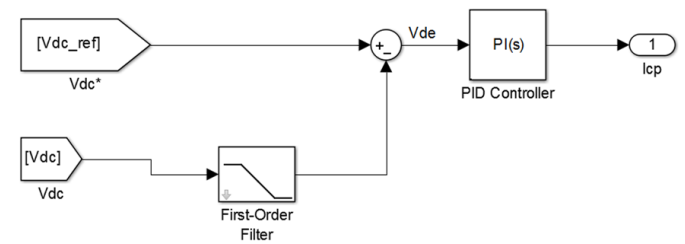


Fig -11: AC loss component generator

- Feed-Forward term:

In favor of for quick dynamic feedback of the system a PV feed forward is imported which is measured by:

$$I_{spv}(n) = \frac{2P_{pv}(n)}{3V_t} \quad \dots\dots\dots (27)$$

Where, P_{pv} is PV power.

The feed forward term generator Simulink model is shown below in Fig-12.

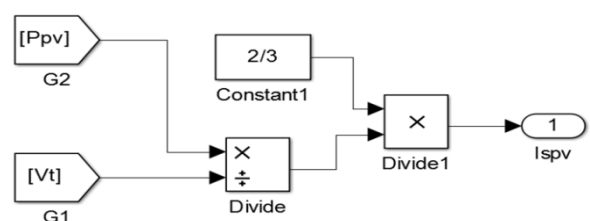


Fig -12: AC loss component generator

5.3 Computation of fundamental components of load currents:

- Fundamental active component (FAC):

The FAC of load current for phase 'a' at the n^{th} instant is given by:

$$i_{pa}(n) = u_{pa}(n) \times 2LPPF[u_{pa}(n) \times \{i_{La}(n) + m \times i_{cpa}(n)\}] \quad \dots\dots\dots (28)$$

Where, $u_{pa}(n)$ is in-phase unit template; $i_{La}(n)$ is load current of phase 'a'; $i_{cpa}(n)$ is the active compensating

current at the n^{th} instant; 'm' is the feedback element (selected between the values 0 to 1, here $m = 0.25$); LPF denotes low pass filter.

The cut-off frequency of LPF is preferred in the range of 15-20 Hz for acquiring less delay in response and remaining harmonics are scaled down through the feedback element 'm'. The value of 'm' is selected within 0 and 1 as it lessens the harmonics percentage in the load current.

For every repetition the value of $i_{cpa}(n)$ (active compensating current) is decreased by means of 'm' and added to the load current there by extremely reducing the harmonics and the value of $i_{cpa}(n)$ is estimated as:

$$i_{cpa}(n) = i_{La}(n) - i_{pa}(n) \quad \dots\dots\dots (29)$$

The Simulink model is as shown in Fig-13.

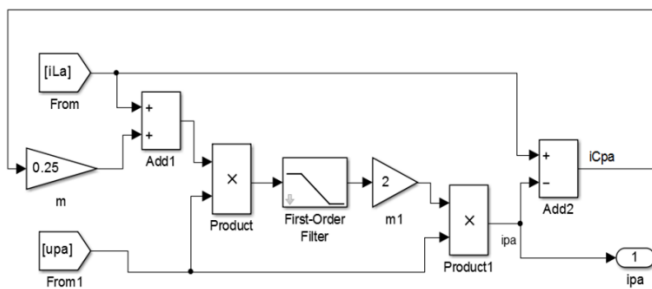


Fig -13: Generation of FAC of load current for phase 'a'

In the same way, the FAC of load current for phase 'b' and phase 'c' at the n^{th} instant are evaluated as:

$$i_{pb}(n) = u_{pb}(n) \times 2LPF[u_{pb}(n) \times \{i_{Lb}(n) + m \times i_{Cpb}(n)\}] \quad \dots\dots\dots (30)$$

$$i_{pc}(n) = u_{pc}(n) \times 2LPF[u_{pc}(n) \times \{i_{Lc}(n) + m \times i_{Cpc}(n)\}] \quad \dots\dots\dots (31)$$

The Simulink models for phase 'b' and phase 'c' is as shown in Fig-14 and Fig-15 respectively.

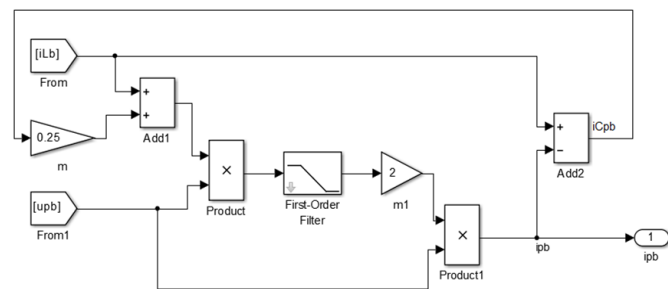


Fig -14: Generation of FAC of load current for phase 'b'

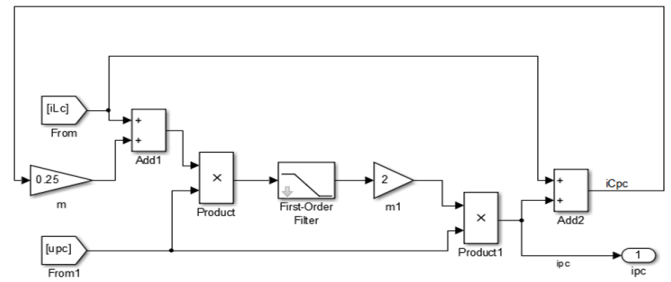


Fig -15: Generation of FAC of load current for phase 'c'

In the same way, the FAC of load current for phase 'b' and phase 'c' at the n^{th} instant are evaluated as:

$$i_{pb}(n) = u_{pb}(n) \times 2LPF[u_{pb}(n) \times \{i_{Lb}(n) + m \times i_{Cpb}(n)\}] \quad \dots\dots\dots (30)$$

$$i_{pc}(n) = u_{pc}(n) \times 2LPF[u_{pc}(n) \times \{i_{Lc}(n) + m \times i_{Cpc}(n)\}] \quad \dots\dots\dots (31)$$

▪ Fundamental reactive component (FRC):

The FRC of load current for phase 'a' at the n^{th} instant is estimated similarly as FAC for phase 'a' as:

$$i_{qa}(n) = u_{qa}(n) \times 2LPF[u_{qa}(n) \times \{i_{La}(n) + m \times i_{Cqa}(n)\}] \quad \dots\dots\dots (32)$$

The value of reactive compensating current ($i_{Cqa}(n)$) is evaluated as:

$$i_{Cqa}(n) = i_{La}(n) - i_{qa}(n) \quad \dots\dots\dots (33)$$

For phase 'b' and phase 'c' the FRC of load currents at the n^{th} instant is evaluated as:

$$i_{qb}(n) = u_{qb}(n) \times 2LPF[u_{qb}(n) \times \{i_{Lb}(n) + m \times i_{Cqb}(n)\}] \quad \dots\dots\dots (34)$$

$$i_{qc}(n) = u_{qc}(n) \times 2LPF[u_{qc}(n) \times \{i_{Lc}(n) + m \times i_{Cqc}(n)\}] \quad \dots\dots\dots (35)$$

The Simulink models for all the three models are as shown in Fig-16, Fig-17 and Fig-18 respectively.

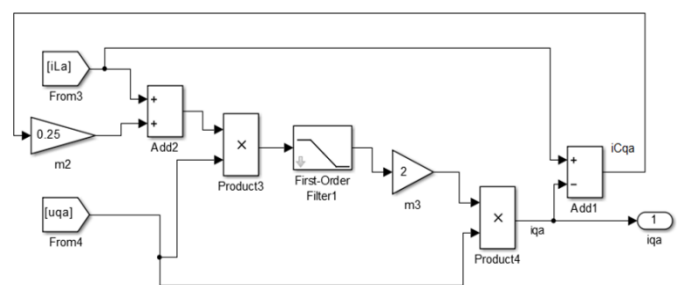


Fig -16: Generation of FRC of load current for phase 'a'

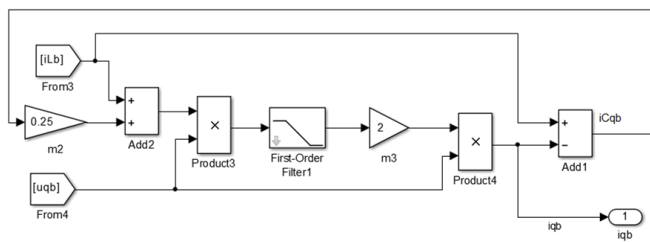


Fig -17: Generation of FRC of load current for phase 'b'

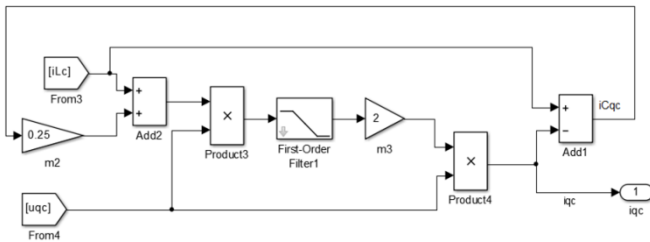


Fig -18: Generation of FRC of load current for phase 'c'

5.4 Production of reference three-phase grid currents:

- Reference value of active component:

The reference value of overall active current component (I_p) of three-phase grid currents is estimated as:

$$I_p = I_{LpA} + I_{cp} - I_{spv} \quad \dots\dots\dots (36)$$

Where, $I_{LpA} = \sqrt{\frac{2}{3}(i_{pa}^2 + i_{pb}^2 + i_{pc}^2)}$ (37)

Simulink model for the generation of I_p is as shown in Fig-19.

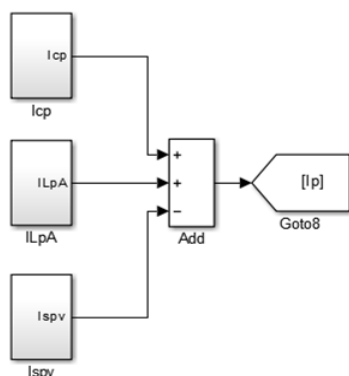


Fig -19: Simulink model for the generation of I_p

The reference values of each of the active component of grid currents are obtained as:

$$i_{pa}^* = I_p \times u_{pa} \quad \dots\dots\dots (38)$$

$$i_{pb}^* = I_p \times u_{pb} \quad \dots\dots\dots (39)$$

$$i_{pc}^* = I_p \times u_{pc} \quad \dots\dots\dots (40)$$

- Reference value of reactive component:

The reference value of absolute reactive component of grid current is obtained as:

$$I_q = I_{cq} - I_{LqA} \quad \dots\dots\dots (41)$$

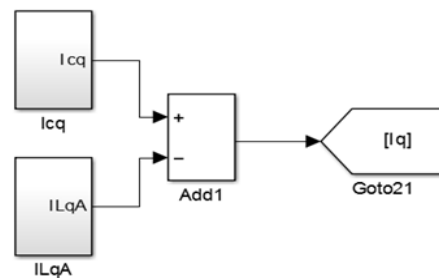


Fig -20: Simulink model for the generation of I_q

- Total reference value of three-phase grid currents:

The net reference values of 3-phase grid currents are estimated as:

$$i_a^* = i_{pa}^* + i_{qa}^* \quad \dots\dots\dots (46)$$

$$i_b^* = i_{pb}^* + i_{qb}^* \quad \dots\dots\dots (47)$$

$$i_c^* = i_{pc}^* + i_{qc}^* \quad \dots\dots\dots (48)$$

5.5 Hysteresis Current control for the generation of gate pulses:

With a view to generate gate signals or pulses so as to turn on the VSI a HCC technique is exercised [18]. The supreme utility of this control scheme is that it can be digitally implemented.

- Working Principle:

Hysteresis controller incorporates a feedback loop which is nonlinear along with hysteresis comparator. In this technique hysteresis comparator includes two levels: lower hysteresis band (LHB) and upper hysteresis band (UHB) [19]. These bands actuate the steady state error. The actual current and the reference current are compared so as to produce any error in the current. This error is then passed to the hysteresis comparator. If the error current reaches UHB, the undermost switches are turned ON and the inductor current decrements thereby

lessening the error current. In a similar way, if the error current reaches LHB the uppermost switches are turned ON and the inductor increments which regulate the current not beyond the limits. This process repeats. Switches work up ON and OFF randomly to trace the reference current and maintain the error current within pre-determined band width.

▪ Design:

The switching frequency of VSI is determined by the subsequent aspects as interpreted in detail below. The configuration of power circuit of 3-phase VSI with R-L load is illustrated in Fig-21.

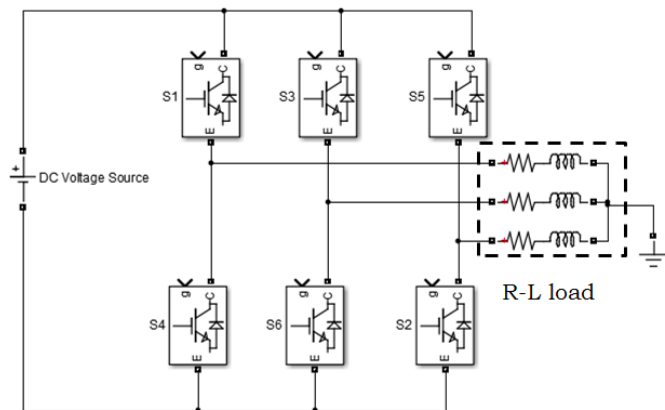


Fig -21: Power circuit of 3-phase VSI

The per phase equivalent circuit of VSI fed with R-L load, when the top switch is stimulated, is depicted in Fig-22. It is defined by the following equation:

$$V_{dc} = R \times I_L + L \frac{dI_L}{dt} \quad \dots\dots\dots (49)$$

Where, V_{dc} is the inverter input voltage; I_L is the load current; R is the resistive load; L is the inductive load;

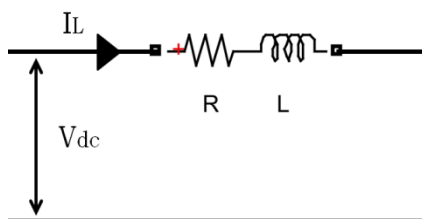


Fig -22: Per phase equivalent circuit of the load

Considering the resistor value to be insignificant, the smallest value of Δt for which the current increments by Δi can be derived by repositioning the eq. (50) as below:

$$L \frac{\Delta i}{\Delta t} = V_{dc} \quad \dots\dots\dots (50)$$

$$\text{But } \Delta t = \frac{T}{2} \quad \dots\dots\dots (51)$$

Where, T is the total time period.

Thus on substitution of eq. (51) in eq. (50) we obtain:

$$f_{s(max)} = \frac{V_{dc}}{2L\Delta i} \quad \dots\dots\dots (52)$$

Where, $f_{s(max)}$ is the maximum switching frequency. This $f_{s(max)}$ can be confined to any value by properly choosing Δi and that is exclusively the band width for an allowed value of load inductance. From eq. (52) inductance value can be calculated if all the other parameters are chosen.

The 3-phase hysteresis controller with three distinct hysteresis comparators is depicted in Fig. 23.

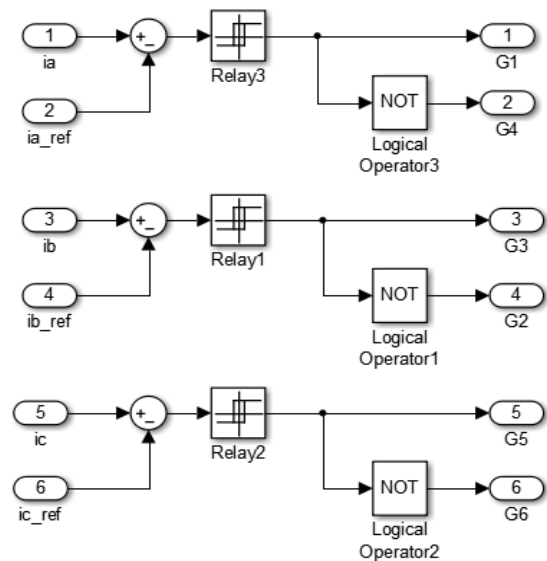


Fig -23: Simulink model of hysteresis current controller

6. SIMULATION RESULTS

6.1 Simulation of PVM

PV cell specifications specified in Table I are employed for modeling purpose. The PVM Simulink model provides the P-V and I-V characteristics. The characteristic curves of P-V and I-V are plotted at nominal temperature for different irradiancies (for 1000W/m², 800W/m² and 600W/m²). Fig-24 and Fig-25 provide the P-V and I-V characteristics curves respectively. The solar insolation profile is as depicted in Fig-26. The simulated waveforms of power, voltage and current of PVM are shown in Fig-27.

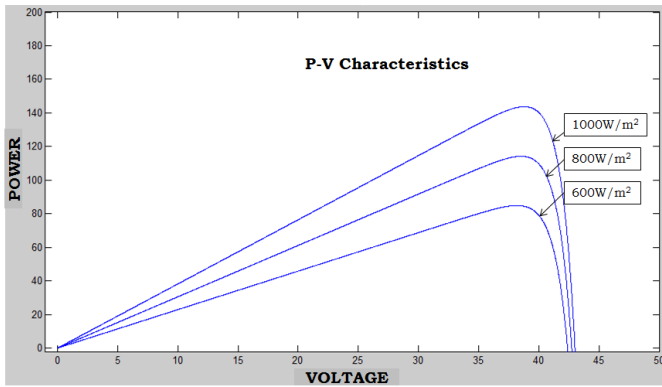


Fig -24: P-V characteristics of PVM

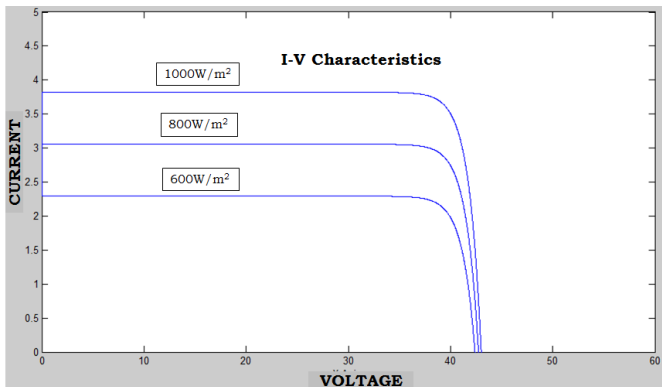


Fig -25: I-V characteristics of PVM

6.2 Simulation of Fuzzy logic MPPT controller:

The fuzzy logic MPPT controller has three subdivisions. First section takes immediate responses of voltage and current from the PV arrangement. It processes and samples the voltage and current values in accordance with the demand of the controller. Second section is the controller with the fuzzy logic. The indicated controller provides the modulation level depending on the control algorithm in order to obtain the maximum power point. The last section is the PWM generator which provides switching gate pulses for the boost converter. The fuzzy logic based MPPT controller scheme is as shown in the Fig-28 and the obtained PWM pulses from the proposed FLMPPT is shown in Fig-29.

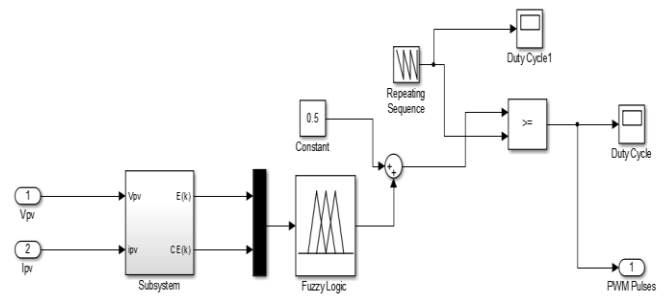


Fig -28: Fuzzy logic controller scheme

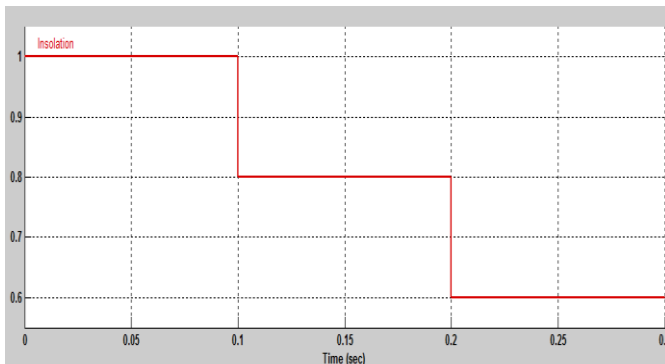


Fig -26: Various insolation levels

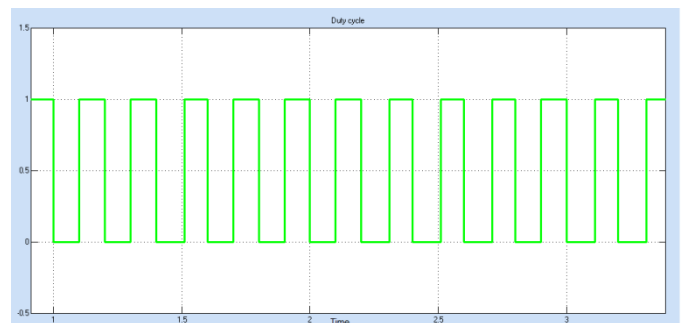


Fig -29: Fuzzy logic controller PWM pulses

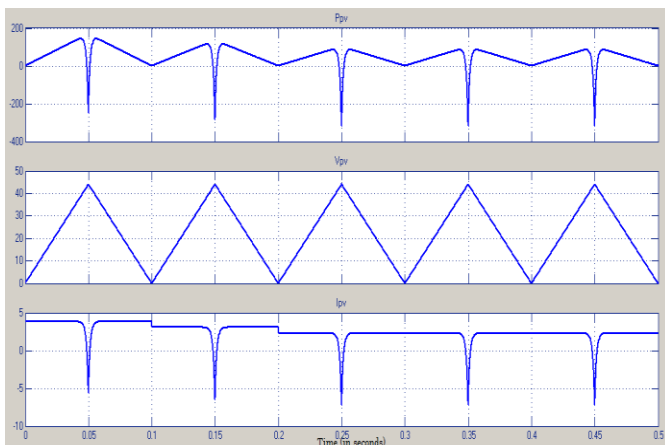


Fig -27: Waveforms of P_{pv} , V_{pv} and I_{pv} of PVM

6.3 Simulation of Boost Converter:

The fuzzy logic MPPT controller provides the gate pulses essential for the boost converter performance. This in turn is necessary for the feeding the VSI. The parameters used for simulation purpose are given in Table III. The output waveform of the boost converter is illustrated in the Fig-30.

Table -3: Boost Converter Parameters Used for the Simulation Purpose

Parameters	Values
Input Voltage	35.62V
Output voltage	200V
Frequency	100kHz
Inductor	485 μ H
Capacitor	1886 μ H

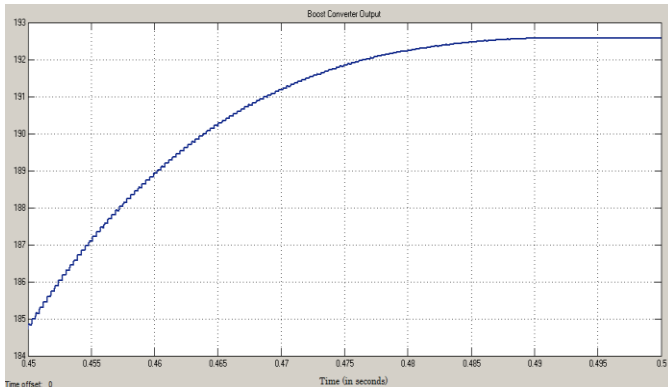


Fig -30: Output of Boost Converter

6.3 Simulation of grid connected VSI:

In any grid connected system, the proposed system voltage must synchronize alongside the grid voltage. In consequence of the above mentioned fact the inverter should work in the grid voltage and frequency. The control strategy consists of the evaluation of: load currents, in-phase and quadrature unit templates, ac and dc loss components and the reference grid currents. The hysteresis regulator and current extractor are used to generate the gate pulses from the reference grid and sensed grid currents so as to operate the VSI. The overall simulation circuit and simulation results of VSI are as depicted in the following figures.

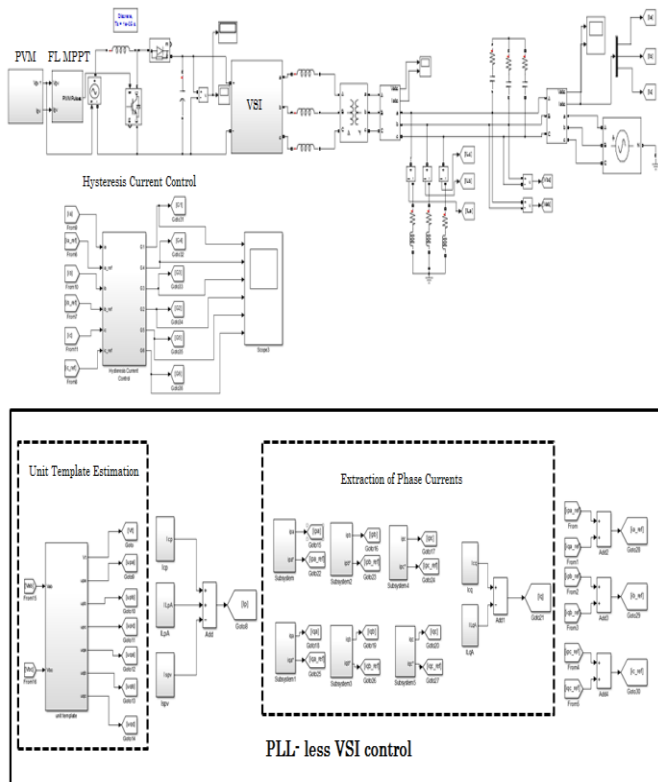


Fig -30: Proposed system Simulink model

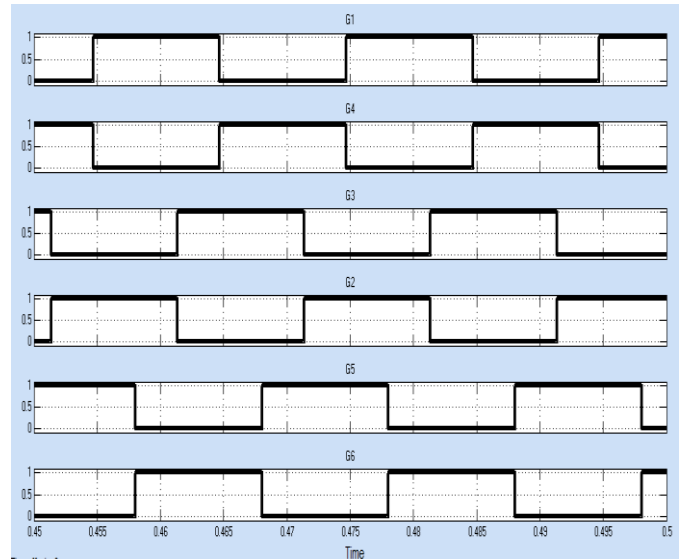


Fig -31: Gate pulses for the VSI from Hysteresis current controller

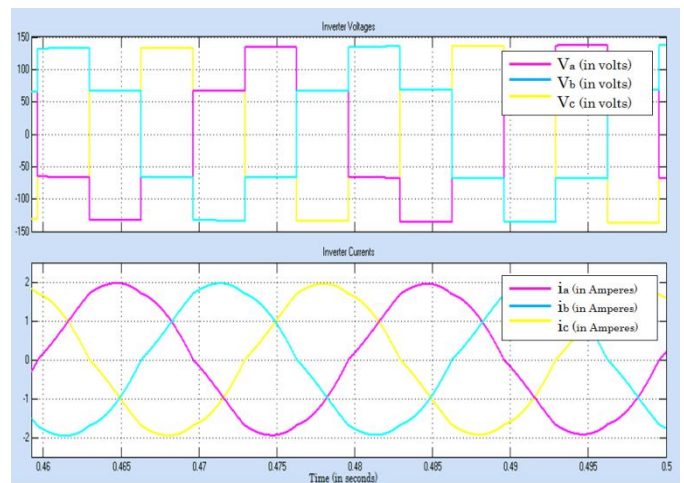


Fig -32: Measured inverter voltages and currents

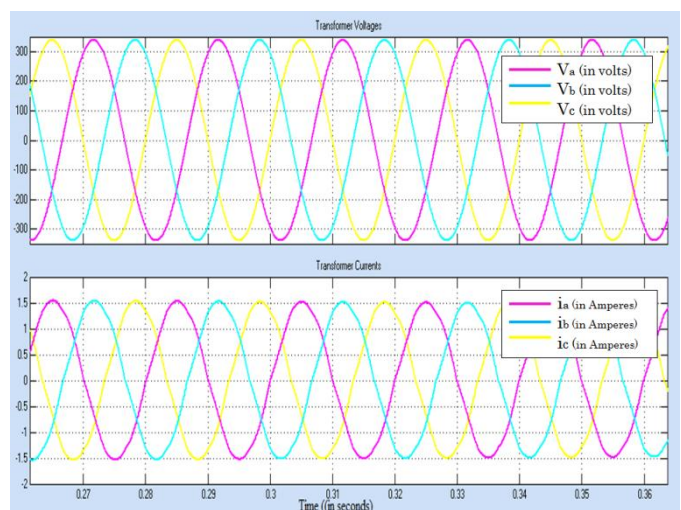


Fig -33: Measured transformer voltages and currents

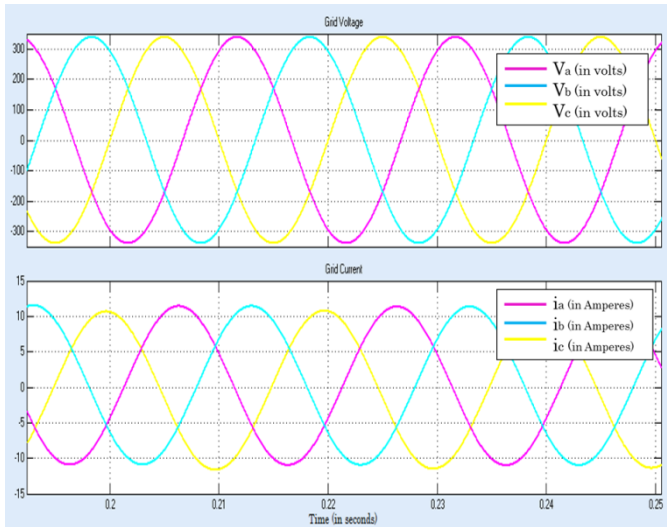


Fig -34: Measured grid voltages and currents

7. CONCLUSIONS

In view of this suggested work a PLL-less based hysteresis current control technique for the three phase Voltage Source Inverter has been designed. The predominant advantages of this technique include easy implementation, elementary and have a speedy response. It also employs the fuzzy logic based MPPT controller for tracking the MPP. Thus it is implied that PV based system evolve into a more productive system with the FLC MPPT. The demonstration of the model has been executed through the simulations in the MATLAB/Simulink environment adopting the sim power system toolbox.

REFERENCES

- [1] B. Subudhi, R. Pradhan, "A comparative study on maximum power point tracking techniques for photovoltaic power systems," *IEEE Trans. on Sust. Energy*, vol. 4, no. 1, Jul. 2012, pp. 89-98.
- [2] S. E. Babaa, M. Armstrong, V. Pickert, "Overview of maximum power point tracking control methods for PV systems," *Journal of Power and Energy Engineering*, vol. 2, Aug. 2014, pp. 59-72.
- [3] Serban. E, Serban.H , "A control strategy for a distributed power generation microgrid application with voltage and current-controlled source converter," *IEEE Trans. Power Electron.*, vol. 25, no. 12, Dec 2010, pp. 2981 – 2992.
- [4] A. Chatterjee, A. Keyhani, D. Kapoor. (2011, July). Thevenin's equivalent of photovoltaic source models for MPPT and power grid studies. Detroit, MI, USA. Presented at Power and Energy Society General Meeting.
- [5] M. G. Villalva, J. R. Gazoli, E. R. Filho, "Comprehensive approach to modeling and simulation of photovoltaic arrays," *IEEE Trans. Power Electron.*, vol. 24, no. 5, May. 2009, pp. 1198-1208.
- [6] H. J. Moller, *Semiconductors for Solar Cells*. Norwood, MA: Artech House, 1993.
- [7] M. Makhlof, F. Messai, H. Benalla, "Modeling and simulation of grid-connected hybrid photovoltaic/battery distributed generation system," *Canadian Journal on Elec. and Electron. Eng.*, vol. 3, no. 1, Jan. 2012.
- [8] N. S. D'Souza, L. A. C. Lopes, X. J. Liu. (2005, June). Recife, Brazil. An intelligent maximum power point tracker using peak current control. Presented at Power Electronics Specialists Conference, 2005. PESC '05. IEEE 36th.
- [9] C. Y. Won, D. H. Kim, S. C. Kim, W. S. Kim and H. S. Kim. (1994, June). A new maximum power point tracker of photovoltaic arrays using fuzzy controller. Presented at 25th Annual IEEE Power Electronics Specialists Conference.
- [10] T. Radjai, L. Rahmani, L. Mekhilef, J. P. Gaubert, "Implementation of a modified incremental conductance MPPT algorithm with direct control based on a fuzzy duty cycle change estimator using Dspace," *Solar Energy*, vol.110, Dec. 2014 pp. 325–337.
- [11] T. J. Ross. "Fuzzy Logic with Engineering Applications," 3rd ed. Chichester, England, United Kingdom: John Wiley & Sons Ltd, 2010.
- [12] A. R. Reisi, M. H. Moradi, S. Jamasb, "Classification and comparison of maximum power point tracking techniques for photovoltaic system: A review," *Ren. and Sust. Energy Reviews*, vol. 19, Mar. 2013, pp. 433-443.
- [13] R. Marouani and A. Mami, "Voltage oriented control applied to a grid connected photovoltaic system with maximum power point tracking technique," *American Journal of Applied Sciences*, vol. 7, 2010.
- [14] G. Pepermans, J. Driesen, D. Haeseldonckx, R. Belmans, "Distributed generation: definition, benefits and issues," *Energy Policy*, vol. 33, no. 6, Apr. 2005, pp. 787-798.
- [15] J. Selvaraj, N. A. Rahim, "Multilevel inverter for grid-connected PV system employing digital PI controller," *IEEE Trans. on Indus. Electr.*, vol. 56, no. 1, Jan. 2009 pp. 149-158.

- [16] R. K. Agarwal, I. Hussain, B. Singh, "Three-phase single-stage grid tied solar PV ECS using PLL-less fast CTF control technique," *IET Power Electronics*, vol. 10, no. 2, Feb. 2017.
- [17] H. Akagi, E. H. Watanabe, M. Aredes. "Instantaneous power theory and applications to power conditioning," 2nd ed. Hoboken, New Jersey, United States: John Wiley & Sons Inc., 2017.
- [18] J. Rodriguez, S. Bernet, P. K. Steimer, "A survey on neutral-point-clamped inverters," *IEEE Trans. on Indus. Electr.*, vol. 57, no. 7, Jul. 2010, pp. 2219-2230.
- [19] D. Kalyanraj, S. L. Prakash, "Design and digital implementation of constant frequency hysteresis current controller for three-phase voltage source inverter using TMS320F2812," *IJPES*, vol. 15, no. 1, Jan. 2014.